INTERNATIONAL JOURNAL FOR NUMERICAL AND ANALYTICAL METHODS IN GEOMECHANICS
Int. J. Numer. Anal. Meth. Geomech., 2007; **31**:1163–1181
Published online 22 November 2006 in Wiley InterScience (www.interscience.wiley.com). DOI: 10.1002/nag.576

Accelerating the convergence of coupled geomechanical-reservoir simulations

L. Jeannin*,†, M. Mainguy, R. Masson and S. Vidal-Gilbert

Institut Français du Pétrole, 1 et 4, avenue de Bois-Préau, F- 92852 Rueil-Malmaison Cedex, France

SUMMARY

The pressure variations during the production of petroleum reservoir induce stress changes in and around the reservoir. Such changes of the stress state can induce marked deformation of geological structures for stress sensitive reservoirs as chalk or unconsolidated sand reservoirs. The compaction of those reservoirs during depletion affects the pressure field and so the reservoir productivity. Therefore, the evaluation of the geomechanical effects requires to solve in a coupling way the geomechanical problem and the reservoir multiphase fluid flow problem. In this paper, we formulate the coupled geomechanical-reservoir problem as a non-linear fixed point problem and improve the resolution of the coupling problem by comparing in terms of robustness and convergence different algorithms. We study two accelerated algorithms which are much more robust and faster than the conventional staggered algorithm and we conclude that they should be used for the iterative resolution of coupled reservoir-geomechanical problem. Copyright © 2006 John Wiley & Sons, Ltd.

Received 21 December 2005; Revised 28 September 2006; Accepted 7 October 2006

KEY WORDS: coupled simulators; iterative algorithms; compaction; petroleum reservoir

1. INTRODUCTION

The oil industry has to face several geomechanical problems such as borehole stability, hydraulic fracturing, reservoir compaction, integrity of bounding seal for acid gas sequestration. Most of the time, these problems involve interactions between fluid flow, heat transfer and mechanics. This is particularly true for production-induced compaction where the interactions between fluid flow and reservoir deformation can be extremely marked. The reservoir compaction is induced by the oil production that lowers the fluid pressure in the reservoir and increases the effective stress on the reservoir rock. The reservoir compaction will be more or less marked depending on the reservoir constitutive law, the pressure change in the reservoir,

*Correspondence to: L. Jeannin, Institut Français du Pétrole, 1 et 4, avenue de Bois-Préau, F- 92852 Rueil-Malmaison Cedex, France.
† E-mail: laurent.jeannin@ifp.fr

reservoir geometry and boundary conditions. Reservoir compaction is a major concern for the oil companies because the stress redistribution associated with the reservoir compaction can trigger well problems like casing collapse or shear failure in the presence of pre-existing faults or weak bedding planes (e.g. Wilmington oil field in California). Surface subsidence (see [1]) is also one of the most visible consequences of the reservoir compaction. Surface subsidence can damage the surface installations (e.g. the Ekofisk oil field) and can also create environmental problem (e.g. the Bachaquero Heavy oil field and Groningen gas field). On the other hand, compaction is a drive mechanism for oil recovery because it reduces the porous volume accessible to the fluids and therefore increases the reservoir production (e.g. the Zuata heavy Oil field in Venezuela).

The stress variations induced by production does not always affect the fluid flows in the reservoir. Nevertheless, for stress-dependent reservoirs, the reservoir compaction significantly modifies the reservoir porosity or permeability so that the fluid flow model cannot be used alone to predict the reservoir production. Therefore, the hydrocarbon production of stress-dependent reservoir requires to couple the fluid flow model with a mechanical model. Such a coupled model has firstly being developed by Biot [2] who proposed a coupled set of equations for describing soil settlement under load. Afterwards, the Biot theory has been extended to multiphase flow in porous media (see e.g. [3]) that can be used to model the production of stress-dependent reservoirs. Two different approaches (see [4]) can be used to solve the coupled set of equations:

- The fully coupled approach uses a single simulator that simultaneously solves the fluid flow and mechanical problems. Consequently, at each time step, the coupled set of equations is solved using a Newton-type method. The fully coupled approach allows full access to the fluid flow and mechanical unknowns so that the coupling between fluid flow and mechanics can be easily operated. However, this approach requires numerous developments to reach the same level of capability as usually encountered in conventional reservoir simulator and conventional stress simulator. For that reason, fully coupled simulators do generally not offer the same level of features as conventional reservoir or stress simulators. In addition, the domain considered in the mechanical problem is larger than the reservoir domain because it includes the reservoir overburden, base and sides. Therefore, the solution cost of the mechanical problem at each reservoir simulator time step can be particularly high in terms of CPU time especially if the fluid flow problem is extended over the reservoir domain.
- The simulator coupling approach relies on an iterative scheme between a fluid flow simulator and a stress simulator. The coupled problem can be solved using iterative algorithms that require the resolution of a fluid flow sub-problem (i.e. a reservoir simulation) and a mechanical sub-problem (i.e. a stress simulation). The iterative algorithm is based on data exchange between the two simulators. If the full convergence of the iterative algorithm is reached, the solution of the simulator coupling approach is the same as the solution of the fully coupled approach using one simulator. However, unlike the fully coupled approach, the simulator coupling approach is more flexible because it benefits from the pre-existing developments of the fluid flow simulator and stress simulator. Furthermore, the simulator coupling approach can be used to reduce the number of mechanical simulation if the coupling algorithm is implemented over time periods that includes several fluid flow time steps.

DOI: 10.1002/nag

Thanks to its flexibility, the coupling approach is being increasingly used by oil and gas companies for analysing the behaviour of stress-dependent reservoirs. Most of the time the coupling is operated through a staggered algorithm between a reservoir simulator and a stress simulator, information being exchanged between the two simulators. First the reservoir simulator provides the pressure changes to the stress simulator. The pressure change is converted into load in the stress simulator that computes in turn the resulting stress and strain changes. Then the stress simulator provides the porosity changes to consider in the reservoir simulation at the next iteration. This process must be iterated until convergence is achieved. The porosity changes assigned to the reservoir simulator can be computed as a function of pressure and geomechanical unknowns (e.g. volumetric strain or mean total stress [5–7]). In the case of single phase linear flow and linear elasticity, the staggered algorithm can be seen as a block Gauss–Seidel iterative method for solving the coupled system [8]. However, it is well known that Gauss–Seidel-type algorithms converge slowly so that the convergence could require a large number of reservoir and geomechanical simulations. Therefore, the staggered coupling algorithm can be extremely computing time consuming, especially for industrial applications and for non-linear reservoir constitutive laws.

Therefore, there is an important need for new coupling algorithms that can significantly improve the convergence rate of the simulator coupling approach. To this aim, this paper presents two algorithms that can be used to solve the coupled fluid flow and deformation problem with two different simulators. The first algorithm is a non-linear gradient conjugate algorithm preconditioned with the stiffness matrix and firstly proposed by Daïm *et al*. [8]. The second algorithm is a non-linear generalized minimum residual method (noted gmres). The paper highlights the differences between these algorithms and the Gauss–Seidel-type algorithm usually used in the simulator coupling approach and explains how these algorithms could be implemented with a reservoir simulator and a stress simulator. Last, the performance of the different algorithms is evaluated on 1D and 3D tests and some recommendations for the choice of the coupling algorithm are proposed.

The content of the paper is as follows: the second section describes mechanical and fluid flow models and examines the coupling between the two models. The next section presents the different algorithms that can be used to iteratively solve the coupled geomechanics-reservoir problem. The first algorithm is the Gauss–Seidel one, commonly applied to couple reservoir-geomechanics simulations. The two other algorithms are the non-linear gradient conjugate method and the non-linear gmres. The last section presents the numerical tests used to compare the iterative algorithms. The comparison is performed in terms of convergence and robustness on a 1D case and on a synthetic reservoir study.

2. GEOMECHANICAL-RESERVOIR COUPLING

2.1. Coupled geomechanics and fluid flow

Let us note that ω is the reservoir domain of the fluid flow model and Ω is the geomechanical domain considered in the mechanical problem. The reservoir domain is embedded in the larger domain Ω that is composed of the reservoir domain with its surrounding formations (reservoir base, sides and overburden). Fluid flow problem only arises in the reservoir domain. The geomechanical domain is large enough so that the boundary conditions for the mechanical

DOI: 10.1002/nag

unknowns are set sufficiently far away from the boundary of the reservoir domain to mimic the *in situ* boundary conditions.

The momentum balance is governed by the mechanical equilibrium equation in both the reservoir and the surrounding formations

$$\operatorname{div}\sigma = f \quad \text{in } \Omega \tag{1}$$

where σ is the total stress tensor and f represents the gravity forces. The strain tensor is the symmetric part of the displacement gradient and is defined by

$$\varepsilon(u) = \tfrac{1}{2}(\nabla u + {}^{\mathrm{t}}\nabla u) \quad \text{in } \Omega \tag{2}$$

where u is the displacement vector. Strain and stress tensors are related through a constitutive law. Assuming a poroelastic behaviour of the reservoir rock and using the continuum mechanics sign convention (compressive stresses are negative), the constitutive law takes the form

$$\sigma = \bar{\bar{C}} : \varepsilon(u) - \alpha P \quad \text{in } \omega \tag{3}$$

where $\bar{\bar{C}}$ is the tensor of the elastic drained coefficients and α is the Biot's coefficient resulting from the definition of the effective stress in porous media and P is the fluid pressure. Assuming an isotropic reservoir rock the elastic tensor is expressed as

$$C_{ijkl} = \frac{Ev}{(1+v)(1-2v)}\delta_{ij}\delta_{kl} + \frac{E}{2(1+v)}(\delta_{ik}\delta_{jl} + \delta_{il}\delta_{jk}) \tag{4}$$

where E and v are the Young's modulus and the Poisson ratio. In the reservoir surrounding formations, the total stress σ is related to the strain tensor with

$$\sigma = \bar{\bar{C}} : \varepsilon(u) \quad \text{in } \Omega\backslash\omega \tag{5}$$

where $\bar{\bar{C}}$ is the tensor of the elastic coefficients of the surrounding formations. Introducing Equation (3) in Equation (1) and taking into account expression (2) of the strain tensor, the mechanical problem can be formulated as a displacement problem that has to be solved with additional initial and boundary conditions.

The fluid flow problem considers two phase fluid flow in the reservoir (oil and water). To simplify, capillary effects are neglected so that the fluid pressure denoted as P of the constitutive law (3) corresponds in the paper to either the oil pressure or the water pressure. The fluid flow in the reservoir domain obeys the generalized Darcy's law in each phase. For compressible fluids, the governing reservoir equations are the mass balance equations of each phase. Assuming no capillary effects, these mass balance equations are given by

$$\begin{cases} \dfrac{\partial}{\partial t}(\rho_{\mathrm{w}} S_{\mathrm{w}}\phi) - \operatorname{div}\left(\rho_{\mathrm{w}}\dfrac{k_{\mathrm{r,w}}}{\mu_{\mathrm{w}}}k(\nabla P - \rho_{\mathrm{w}}\mathbf{g})\right) = q_{\mathrm{w}}\delta(x = x_{\mathrm{well}}) \\ \dfrac{\partial}{\partial t}(\rho_{\mathrm{o}} S_{\mathrm{o}}\phi) - \operatorname{div}\left(\rho_{\mathrm{o}}\dfrac{k_{\mathrm{r,o}}}{\mu_{\mathrm{o}}}k(\nabla P - \rho_{\mathrm{o}}\mathbf{g})\right) = q_{\mathrm{o}}\delta(x = x_{\mathrm{well}}) \end{cases} \quad \text{in } \omega \tag{6}$$

where subscript o refers to the oil phase and subscript w to the water phase. In Equation (6), x and t refer to the space and time variables, respectively, and ϕ and k denote the reservoir porosity and permeability, respectively. Still in Equation (6) and for $i = \mathrm{w}$ and o, S_i is the saturation of phase i, $k_{\mathrm{r},i}(S_{\mathrm{w}})$ is the relative permeability of phase i, μ_i is the dynamic viscosity of phase i, $\rho_i(P)$ is the density of phase i and q_i is the volumetric rate of source term in phase i at the location $x = x_{\mathrm{well}}$.

DOI: 10.1002/nag

The coupling between the fluid flow model and the mechanical model can be highlighted using the pressure and porosity variables. According to Equations (1) and (3), the pressure changes in the reservoir lead to a stress redistribution and strain changes in the geomechanical domain. The strains localized in the reservoir domain can modify the reservoir porosity, appearing in Equation (6). Using the second constitutive law of poroelasticity [9], the porosity change for a single phase flow can be related to the volumetric strain and the pressure change according to this following equation:

$$\frac{\partial \phi}{\partial t} = \alpha \frac{\partial}{\partial t}(\operatorname{div} u) + \frac{1}{\eta}\frac{\partial P}{\partial t} \quad \text{in } \omega \tag{7}$$

where η is a reservoir rock property independent of the fluid properties and that can be expressed as a function of the Biot's coefficient, the porosity and K_s is the bulk modulus of the solid phase of the porous rock

$$\frac{1}{\eta} = \frac{(\alpha - \phi)}{K_s} \tag{8}$$

Moreover, the following identities are verified [9]:

$$\alpha = 1 - \frac{K_d}{K_s} \quad \text{and} \quad K_d = \frac{E}{3(1-2v)}$$

where k_d the rock-drained bulk modulus.

For a reservoir rock composed of incompressible grains ($k_s = \infty$), the biot's coefficient equals one and the right hand side of Equation (8) vanishes so that Equation (7) reduces to

$$\frac{\partial \phi}{\partial t} = \frac{\partial}{\partial t}(\operatorname{div} u) \quad \text{in } \omega \tag{9}$$

This last equation shows that, for an incompressible solid phase, the porosity change is equal to the volumetric strain rate. In this case, the mass change of fluid per unit of volume writes

$$\frac{\partial \rho \phi}{\partial t} = \left(\rho \frac{\partial}{\partial t}(\operatorname{div} u) + \phi c_{\mathrm{fl}} \rho_{\mathrm{ref,fl}} \frac{\partial P}{\partial t}\right)$$

$$\text{with } \rho = \rho_{\mathrm{ref,fl}}(1 + \phi c_{\mathrm{fl}}(P - P_{\mathrm{ref}}))$$

where $\rho_{\mathrm{ref,fl}}$ is the fluid density at reference pressure p_{ref} and c_{fl} is the fluid compressibility.

In the case of two phase flow (with $i = \mathrm{w}$ and o), the mass change per unit of volume per phase writes

$$\frac{\partial S_i \rho_i \phi}{\partial t} = \left(\rho_i S_i \frac{\partial}{\partial t}(\operatorname{div} u) + \phi c_{\mathrm{fl}_i} \rho_{\mathrm{ref,fl}_i} S_i \frac{\partial P}{\partial t} + \rho_i \phi \frac{\partial S_i}{\partial t}\right)$$

where $\rho_i = \rho_{\mathrm{ref,fl}_i}(1 + \phi c_{\mathrm{fl}_i}(P - P_{\mathrm{ref},i}))$ with $\rho_{\mathrm{ref,fl}_i}$ is the density of fluid i at reference pressure $P_{\mathrm{ref},i}$ and c_{fl_i} the fluid compressibility of fluid i.

Note that the following coupling algorithms and numerical examples are presented under the assumption of a reservoir rock composed of incompressible grains and for which Equation (9) holds. However, the coupling algorithms can be easily extended to the case of compressible grains by considering that the first term is the right hand side of (7) can be handled as in the case of an incompressible solid matrix and that the second term in the right hand side of (7) can be managed as a compressibility in the reservoir simulator.

DOI: 10.1002/nag

2.2. Time and space discretizations

Finite volume schemes are generally used for the reservoir spatial discretization to ensure mass conservation in each cell and an efficient discretization of the hyperbolic and parabolic terms in the flow equations. The finite volume scheme is obtained by integrating the mass balance equations of each phase (i.e. Equations (6)) on each cell of the finite volume mesh as prescribed by finite volume techniques. An upwind scheme has been used to evaluate the hyperbolic terms of the equations (see [10]). Concerning the time integration, a semi-implicit method named implicit pressure explicit saturation (IMPES) has been implemented.

The displacement problem is an elliptic one for the displacement vector u and is solved using the finite element method. The stress equilibrium equation is discretized using a weak form of the equilibrium equations and quadratic functions as basis functions (see e.g. [11]). The choice of quadratic functions for the displacement vector and of constant functions for the pressure and saturation on each cell ensures the compatibility conditions that are necessary and sufficient for the convergence of the scheme [12, 13].

The discretized forms of the fluid flow and mechanical equations are given by Daïm *et al.* [8] and lead to a system of equations [4,5] given by

$$\begin{pmatrix} C & B' \\ -B & A \end{pmatrix} \begin{pmatrix} P^{n+1} \\ u^{n+1} \end{pmatrix} = \begin{pmatrix} G \\ F \end{pmatrix} \tag{10}$$

where P^{n+1} is a vector of size N that contains the pressure unknowns at time t^{n+1} for all cells of the finite volume mesh and u^{n+1} is a vector of size M that contains the displacement unknowns of the finite element methods at time t^{n+1}. Note that, for a sake of clarity, the saturation unknown vector does not appear in the system (10) because the saturation does not directly act on the stress equilibrium. In system (10), A is the stiffness matrix of dimension $M \times M$ that accounts for linear elasticity of the displacement problem, whereas C is the reservoir non-linear operator ($\mathbb{R}^N \to \mathbb{R}^N$) associated to the fluid flow problem. B and B' are, respectively, an $N \times M$ and an $M \times N$ rectangular matrices that account for the coupling between displacement and fluid flow unknowns. In the framework of poroelasticity, we have $B' = {}^{\mathrm{t}}B$. The matrix B allows to compute the variation of pore volume for each finite volume cell K (with volume $m(K)$) using

$${}^{\mathrm{t}}B[u_l^{n+1} - u_l^n]_{l=1,\ldots,M} = [m(K)\Delta\phi_K]_{K=1,\ldots,N} = \left[\int_K (\operatorname{div} u^{n+1} - \operatorname{div} u^n)\,\mathrm{d}x\right]_{K=1,\ldots,N} \tag{11}$$

The right hand side of system (10) is composed of the gravity loading term F and the reservoir source term G. These terms depend on the pressure and displacement unknowns computed at the previous step (i.e. P^n and u^n).

3. ALGORITHMS FOR SIMULATOR COUPLING

This section presents three algorithms that can be used to solve the coupled set of equations (10) with a reservoir simulator in conjunction with a stress simulator. The first algorithm is a staggered coupling algorithm that consists of iterative resolutions of reservoir and stress simulations over a time increment. This algorithm is the one generally used for coupled reservoir-geomechanics simulations [4, 5, 14].The second algorithm is a non-linear gradient

DOI: 10.1002/nag

conjugate algorithm preconditioned with the stiffness matrix and firstly proposed by Daïm *et al.* [8]. The third algorithm is a non-linear gmres.

3.1. Staggered sequential algorithm

In the staggered sequential algorithm, the coupled set of equations (10) is solved using a sequence of one reservoir simulation followed by one stress simulation. To illustrate the algorithm principle, let us assume that the pressure and displacement vectors have been computed at time t^n and that we want to compute the pressure and displacement vectors at the next time t^{n+1}. The staggered algorithm starts with a reservoir simulation that provides the pressure change $P^{1,n+1} - P^n$ at the first iteration between times t^n and t^{n+1}. This pressure change affects the stress equilibrium through the term $B(P^{1,n+1} - P^n)$. Using this term as a load in the displacement problem, the stress simulator computes the new displacement vector $u^{1,n+1}$ that results from the pressure change in the reservoir computed at the first iteration. The displacement increment $u^{1,n+1} - u^n$ leads to porosity changes that affect the fluid flow. The porosity change computed by the stress simulator is taken into account in the fluid flow model by using the term ${}^{\mathrm{t}}B(u^{1,n+1} - u^n)$ as a load in the next reservoir simulation at iteration 2. This process is iterated until full convergence of the pressure and displacement unknowns and the staggered coupling algorithm is provided by:

Staggered coupling algorithm:

Initialization of $\Delta\phi^1$

For $l = 1, 2 \ldots$ *until convergence Do*

Calculate $P^{l,n+1}$ *taking into account* $\Delta\phi^l$	Reservoir Simulation
Calculate $u^{l,n+1}$ *using* $P^{l,n+1}$ *as a load*	Stress Simulation
Calculate $\Delta\phi^{l+1}$ *using* (11)	

End do

Reservoir simulators generally use a rock compressibility parameter in the porosity–pressure law. The linear porosity–pressure law of the reservoir simulator takes the form

$$\phi = \phi_0(1 + c_{\mathrm{r}}(p - p_0)) \tag{12}$$

where p_0 and ϕ_0 are references values of the pressure and porosity and c_{r} is the rock compressibility parameter of the reservoir simulator. This rock compressibility takes into account the pore volume change due to the reservoir compaction in the reservoir simulator. However, it is recognized that such a parameter cannot provide a full representation of the stress change induced by the reservoir compaction (see e.g. [15]). Actually, the rock compressibility parameter used in conventional reservoir simulator provides a simplified geomechanical approach that remains valid under limiting assumptions and specific reservoir stress paths (see [5]). The staggered algorithm given above holds for a null reservoir rock compressibility but can be extended for strictly positive reservoir rock compressibility. In that case, the porosity correction to be used in the algorithm must be corrected from the porosity change already accounted for in the reservoir simulator due to the reservoir compressibility such that (11) becomes

$$m(K)(\Delta\phi_K + \phi_K^n c_{\mathrm{r}}(p_K^{n+1} - p_K^n)) = \int_K (\operatorname{div} u^{n+1} - \operatorname{div} u^n)\,\mathrm{d}x \tag{13}$$

DOI: 10.1002/nag

Bévillon and Masson [16] have shown that the reservoir rock compressibility c_r is useful to ensure the unconditional stability of the staggered algorithm and that the smallest compressibility ensuring stability is the best parameter. In the case of a linear reservoir problem, system (10) is a linear system of equations and the staggered algorithm can be interpreted as a Gauss–Seidel algorithm with a relaxation parameter equal to $(1 + c_r/c_f)^{-1}$ where c_f is the fluid compressibility [8]. Therefore, the rock compressibility parameter c_r introduced in the reservoir simulator can be considered as a numerical parameter that has to be chosen to improve the convergence rate of the staggered algorithm.

The staggered algorithm has been implemented using reservoir and stress simulators. As described in Section 2.2, a reservoir finite volume simulator is used in conjunction with a finite element stress simulator. The convergence criterion is based on the L^2 norm of normalized pressure and displacement fields. Note that this algorithm requires, at each iteration, one reservoir simulation followed by one mechanical simulation. This algorithm can be easily extended to the case of a reservoir rock composed of compressible grains (i.e. $c_s > 0$) and for which the Biot's coefficient is lower than one (i.e. $\alpha < 1$). In that case, an alpha factor appears in the coupling operator B and the reservoir rock matrix compressibility c_s is handled in the reservoir simulator using an additional compressibility equal to $1/(\phi_0 \eta)$. As the Gauss–Seidel-type algorithms converge slowly, two other algorithms based on more advanced techniques for the resolution of the coupled system (10), are proposed.

3.2. Non-linear preconditioned conjugate gradient algorithm

The conjugate gradient algorithm is an efficient algorithm for solving linear system of equations with symmetric positive definite matrix. Daïm *et al.* [8] propose to apply this algorithm to the second equation of system (10) in which the pressure is seen as a function of the displacement according to the first equation of system (10). Therefore, the pressure unknown P^{n+1} is expressed as a function of the displacement unknown u^{n+1} using a non-linear operator R depending on the reservoir operator C, the reservoir source term G and the coupling matrix B

$$P^{n+1} = R({}^{t}Bu^{n+1}) \tag{14}$$

This last equation is introduced into the first equation of system (10) to give a non-linear system of equations for which the main unknown is u^{n+1}. Let us note that L is the non-linear operator associated to this system, the displacement problem takes the form

$$Au^{n+1} - B(R({}^{t}Bu^{n+1})) = L(u^{n+1}) = F \tag{15}$$

In the case of single phase flow, R is a linear operator so that Equation (15) turns to be a linear system of equations with L a symmetric positive definite matrix. This linear system (15) can be solved using the conjugate gradient method. The natural preconditioner matrix for Equation (15) is the inverse of the stiffness matrix (i.e. A^{-1}). Conjugate gradient method has been developed for symmetric positive definite linear system but can be extended to non-linear systems with symmetric positive definite Jacobian matrices. However, in the case of multiphase flows, Equation (15) does not derive from a potential and the Jacobian matrix associated to the non-linear operator L is *a priori* non-symmetric and non-positive definite. However, lack of robustness of the conjugate gradient algorithm

DOI: 10.1002/nag

due to non-symmetry and non-positivity of the Jacobian matrix has not been observed on numerical tests.

Using the inverse of the stiffness matrix as preconditioner, the non-linear preconditioned conjugate gradient algorithm used for the resolution of Equation (15) is described below [8]

Preconditioned conjugate gradient algorithm:

Choose u_0
Compute $r_0 = F - L(u_0)$, $z_0 = A^{-1}r_0$, *and* $d_0 = z_0$
For $l = 0, 1 \ldots$ *until convergence Do*

$P' = R({}^{t}B(u_l + \varepsilon d_l))$	Reservoir simulation
$y_l = Ad_l - B(P' - P_l)/\varepsilon$	Stress residual computation
$\alpha_l = (r_l, z_l)/(y_l, d_l)$	
$u_{l+1} = u_l + \alpha_l d_l$	
$P_{l+1} = R({}^{t}B(u_{l+1}))$	Reservoir simulation
$r_{l+1} = F - Au_{l+1} + BP_{l+1}$	Stress residual computation
$z_{l+1} = A^{-1}r_{l+1}$	Stress simulation
$\beta_l = (r_{l+1}, z_{l+1})/(r_l, z_l)$	
$d_{l+1} = z_{l+1} + \beta_l d_l$	

End Do

At each iteration, the computation cost of the non-linear preconditioned conjugate gradient algorithm is given by two reservoir simulations, one mechanical simulation and two stress residual computations. The evaluation of the mechanical residual is always negligible compared to the inversion of the mechanical operator (sress simulation). It is important to note that the previous form of the preconditioned conjugate gradient algorithm requires that matrices A and B can be extracted from the mechanical or reservoir simulator to compute the stress residue. However, this is not always the case with industrial simulators so that one could prefer to apply the gradient conjugate method without preconditioning to the following fixed point problem:

$$u^{n+1} - A^{-1}(B(R({}^{t}Bu^{n+1})) - F) = u^{n+1} - H(u^{n+1}) = 0 \tag{16}$$

operator H formally corresponds to a reservoir simulation followed by a mechanical simulation. when the gradient conjugate method is directly applied to Equation (16) instead of Equation (15), two reservoir simulations and two stress simulations (one for the Jacobian matrix evaluation and one for the residual evaluation) are needed per iteration.

3.3. Non-linear gmres algorithm

The non-linear gmres algorithm (see [17]) is a robust method adapted to the resolution of non-linear fixed point problems. Like conjugate gradient algorithm, the gmres algorithm is based on projection on affine Krylov subspace (the subspace of Krylov of index k associated to the initial residue r_0 of the linear system $Ax = b$ is generated by $(r_0, Ar_0, A^2r_0, \ldots, A^kr_0)$). However, in contrast with the conjugate gradient algorithm, the non-linear gmres algorithm does not suppose that the Jacobian matrix is symmetric positive definite. Therefore, this method appears to be more adapted than the conjugate gradient method to the resolution of systems (15) or (16) that can lead to non-symmetric and non-positive definite Jacobian matrix in practical situations.

DOI: 10.1002/nag

The gmres algorithm is applied to the non-linear fixed point problem given by Equation (16). The most important steps of the algorithm are

Non-linear gmres algorithm:

Choose u_0
Calculate $H(u_0)$ Stress & reservoir simulations
For $l = 0, 1 \ldots$ *until convergence Do*
Computation of the residue $r_l = u_l - H(u_l)$
$v_1 = r_l / \|r_l\|$
$\beta_l = \|r_l\|$
Step 1: *Building an orthonormal base* $(v_i)_{i=1\ldots j}$ *of the Krylov space* K_l *of dimension* j *using Arnoldi algorithm*
$j = 0$
Do
$j = j + 1$
$w_j = v_j - [H(u_l + \varepsilon v_j) - H(u_l)]/\varepsilon$ Stress & reservoir simulations
Do $i = 1, 2 \ldots j$
$h_{ij} = (w_j, v_i)$
End Do
$v_{j+1} = w_j - \Sigma_{i=1,\ldots j}\, h_{ij} v_i$
$v_{j+1} = v_{j+1} / \|v_{j+1}\|$
Compute $\rho = \|u_l - H(u_l) + \delta u_l^j - H'(u_l)\delta u_l^j\|$ *without evaluating* δu_l^j
while $\rho > \varepsilon'$
Step 2: *Computation of the approached solution*
Define the matrix $V_j = [v_1, v_2 \ldots v_j]$
Define H_j *the upper matrix of dimension* $(j + 1 \times j)$ *of coefficients* (h_{ij}) *computed at step* 1
Find y_j *that minimizes* $\|\beta_l e_1 - H_j y\|_2$ *with* $(e_1 = (1, 0 \ldots 0)$ *of dimension* $j + 1)$
$\delta u_l^j = V_j y_j$
$u_{l+1} = u_l + \delta u_l^j$
Compute $H(u_{l+1})$ Stress & reservoir simulations
if $\|u_{l+1} - H(u_{l+1})\| < \varepsilon''$
convergence
else
$l = l + 1$
End Do

As previously mentioned for the conjugate gradient algorithm, the non-linear operator H requires one reservoir simulation followed by one stress simulation. Because the size of the Krylov space used at each iteration is variable, the number of reservoir and stress simulations per iteration is *a priori* not known. However, the number of reservoir and stress simulations remains equal in any cases.

4. ALGORITHM COMPARISON

The three coupling algorithms described in the previous section have been implemented using a reservoir finite volume simulator in conjunction with a finite element stress simulator. The coupling between the reservoir and stress simulators is not operated at each time step of the fluid

DOI: 10.1002/nag

flow model but on time periods that contain several time steps. This makes possible to keep small time steps in the reservoir simulation (this is necessary to ensure an accurate approximation of reservoir unknowns) and to reduce the number of stress simulations on one coupling period. Indeed, the computing cost of a stress simulation is usually larger than the computing cost of a reservoir simulation. Therefore, the displacement is computed at time $T_0, T_1, \ldots, T_f$ where the time period (or the coupling period) between two stress simulations (i.e. $T_{k+1} - T_k$) is composed of several reservoir time steps.

This section compares the staggered algorithm, the preconditioned conjugate gradient algorithm and the non-linear gmres algorithm on 1D and 3D tests. The first test models 1D water flooding in rock, whereas the second test simulates a more realistic reservoir production. The first test also analyses the role of the pore compressibility factor used in the reservoir simulator.

4.1. 1D water flooding

In that first test, the reservoir and geomechanical domains are superimposed and correspond to a column of 40 m high with a square cross-section of 1 m per 1 m.

For the reservoir simulation approach, the reservoir domain is initially saturated with oil. At time $t = 0$, water is injected at constant flow rate at the basis of the reservoir domain, whereas oil is produced at constant pressure at the top of the reservoir domain. The relative permeability of the fluid flow model follows quadratic laws given by

$$k_{rw}(S_w) = S_w^2, k_{ro}(S_w) = (1 - S_w)^2 \tag{17}$$

and oil and water are supposed to be compressible according to the equation of state defined in Section 2.1. The petrophysical properties of the fluid flow model together with the initial and boundary conditions are given in Table I.

For the geomechanical modelling approach, the geomechanical domain is the same as the reservoir domain and is assumed to behave as an isotropic poroelastic medium. Uniaxial strain

Table I. Fluid flow and mechanical parameters.

Fluid flow	
Initial porosity	0.1
Reservoir permeability	5×10^{-13} m^2
Oil viscosity	5×10^{-3} Pa s
Water viscosity	1×10^{-3} Pa s
Oil compressibility	4×10^{-10} Pa^{-1}
Water compressibility	4×10^{-10} Pa^{-1}
Initial oil density	1
Initial water density	1
Initial pressure	0.1 MPa
Pressure at the production well	10 MPa
Water flow rate	8.64 m^3 days^{-1}
Stress	
Young's modulus	$5.333 \times 10^{+2}$ MPa
Poisson ratio	0.333
Biot's coefficient	1

DOI: 10.1002/nag

conditions are imposed without any displacement in the x and y-directions and the strain only occurs in the z-direction. According to these assumptions, the vertical stress σ_z is related to the fluid pressure and to the vertical strain ε_z, by (initial pressure and vertical stress are null)

$$\sigma_z = K_{\text{uni}}\varepsilon_z - \alpha P \tag{18}$$

where K_{uni} is the bulk modulus in uniaxial conditions and can be related to the Young's modulus E and Poisson ratio v using

$$K_{\text{uni}} = \frac{E(1-v)}{(1-2v)(1+v)} \tag{19}$$

Table I gives the values of the mechanical parameters used for the present test. Next, the coupling algorithms are compared using two boundary conditions for the mechanical problem

- The first boundary condition (case 1) assumes that the vertical load is constant (i.e. oedometric condition). In that case, the volumetric strain equals the vertical strain and is proportional to the pressure change according to Equation (18). As a consequence, the poroelastic system of equations can be decoupled and the porosity change given by Equation (7) is proportional to the pressure change

$$\frac{\partial}{\partial t}\phi = \left(\frac{\alpha^2}{K_{\text{uni}}} + \frac{1}{\eta}\right)\frac{\partial}{\partial t}P \tag{20}$$

  Therefore, with that particular boundary condition, it is possible to compute an equivalent reservoir compressibility from (20) that can be used in the reservoir simulator to solve the reservoir problem without running the stress simulation. The reservoir compressibility deduced from (20) is the oedometric compressibility expressed by

$$c_{\text{r}} = c_{\text{oedo}} = \frac{1}{\phi}\left(\frac{\alpha^2}{K_{\text{uni}}} + \frac{1}{\eta}\right) \tag{21}$$

- The second boundary condition (case 2) supposes that the vertical displacement is imposed at the top and at the bottom of the geomechanical domain. Therefore, in that case, the porosity change depends not only on the pore pressure change but also on the vertical stress variation (using Equations (7) and (19))

$$\frac{\partial\phi}{\partial t} = \frac{\alpha^2}{K_{\text{uni}}}\frac{\partial\sigma_z}{\partial t} + \left(\frac{\alpha^2}{K_{\text{uni}}} + \frac{1}{\eta}\right)\frac{\partial P}{\partial t} \tag{22}$$

  Therefore, this case requires the computation of the vertical stress. Assuming no body forces, the stress equilibrium shows that the vertical stress does not depend on the vertical co-ordinate. Therefore, Equation (18) is integrated along z to express the vertical stress of the form:

$$L\sigma_z = K_{\text{uni}}(u_z(z=L) - u_z(z=0)) - \alpha\int_{z=0}^{L} p(z)\,\mathrm{d}z \tag{23}$$

This last equation shows that the vertical stress depends on the boundary conditions and on the whole pressure change in the reservoir domain. As a result, the vertical stress is not proportional to the local pressure change so that the porosity change cannot be deduced from the pressure

DOI: 10.1002/nag

change using an equivalent reservoir compressibility. Therefore, in that case it is necessary to couple the fluid flow model with the mechanical model to correctly solve the problem. In what follows, the total vertical displacement variation along the geomechanical domain is assumed to be null (i.e. $u_z(z = L) - u_z(z = 0) = 0$).

Reservoir and geomechanical domains are discretized using 40 cells of 1 m high. The geomechanical simulations are performed over ten periods of 10^3 s, each period been divided into five reservoir time steps. The convergence criterion of the three iterative algorithms assumes that the relative variation of the pressure and displacement between two consecutive iterations is less than 5×10^{-5} (using the quadratic norm). The epsilon parameter of the non-linear gmres and preconditioned conjugate gradient algorithm allowing the evaluation the Jacobian matrix was adjusted, after some tests, to 10^{-4}. Moreover, we verify the accuracy of the results obtained with the different algorithms. The normalized L^∞ norm of the relative difference of the pressure and displacement solution fields obtained for the three different algorithms was lower than 10^{-4}.

Table II compares the iteration numbers of the three algorithms on the 1D test for constant vertical load (i.e. case 1) and constant vertical displacement (i.e. case 2). For both cases, the staggered algorithm has been tested using no reservoir compressibility in the reservoir simulation (i.e. $c_r = 0$) and using a reservoir compressibility equal to the oedometric compressibility in the reservoir simulation (i.e. $c_r = c_{oedo}$ given by Equation (21)). Because the gmres algorithm requires a variable number of stress (and reservoir) simulations per iteration, the comparison is performed in terms of number of stress simulations for each period of coupling (i.e. $T_{k+1} - T_k$). Table II gives the mean value of the number of stress simulations per period of coupling for all algorithm and boundary conditions. The mean number of reservoir simulations per coupling period is given between parentheses in the same table after the mean number of stress simulations. According to the algorithms presented in Section 3, the number of reservoir simulations is equal to:

- the number of stress simulations for the staggered algorithm;
- twice the number of stress simulations for the preconditioned conjugate gradient algorithm;
- the number of stress simulations for the gmres algorithm.

The test performed with the staggered algorithm first underlines the role of the reservoir compressibility to allow the convergence of this algorithm. Actually, the ratio of the rock compressibility and the fluid compressibility is particularly critical (due to the low value of young's modulus we have chosen—see [16]) so that the staggered algorithm with no relaxation parameter does not converge for both boundary conditions (i.e. cases 1 and 2). On the contrary, when the oedometric compressibility is used as a relaxation parameter in the reservoir simulator, the staggered algorithm converges. In case 1, where the rock compressibility represents exactly

Table II. Comparison of the mean number of stress simulations per period of coupling.

	Staggered algorithm with no reservoir compressibility	Staggered algorithm with oedometric compressibility	Preconditioned conjugate gradient	Non-linear gmres
Case 1	No convergence	2 (2)	7 (14)	10.6 (10.6)
Case 2	No convergence	28.5 (28.5)	5.6 (11.2)	7.2 (7.2)

DOI: 10.1002/nag

the porosity change due to rock strain, the Gauss–Seidel converges in two iterations. Convergence also occurs in case 2, but the benefit of the reservoir compressibility remains weak because the number of stress simulations is high. Furthermore, the rate of convergence appears to be extremely sensitive to the choice of the reservoir compressibility. For example, the mean number of stress simulations increases from 2 to 9 when the reservoir compressibility increases to one and half of the oedometric compressibility, for case 1.

Table II also shows that the conjugate gradient algorithm and the gmres algorithm are robust algorithms that converge for both cases. The interesting case is the second one for which a real coupling exists between the fluid flow and displacement models. For that case, the preconditioned conjugate gradient algorithm converges 5 times faster than the staggered algorithm, whereas the gmres algorithm converges 4 times faster than the staggered algorithm. Therefore, the preconditioned conjugate gradient algorithm appears to be the most interesting algorithm. However, as previously mentioned, the preconditioned conjugate gradient algorithm requires a full access to the stiffness and coupling matrix in the stress simulator. Because this is not always possible with commercial finite element stress simulator, the other formulation of the conjugate gradient algorithm without preconditioning has also been tested. Using such an algorithm, the mean number of stress simulations per coupling period increases:

- from 7 (with 14 reservoir simulations) to approximately 15 (with the same number of reservoir simulations) for case 1;
- from 5.6 (with 11.2 reservoir simulations) to 11.2 (with the same number of reservoir simulations) for case 2.

Therefore, if the stiffness and coupling matrix are not available in the stress simulator, the performance of the gmres algorithm becomes better than the conjugate gradient algorithm applied to the fixed point problem (16) with no preconditioner.

4.2. 3D reservoir production case

To study a more realistic 3D case, we perform coupled simulations with two industrial simulators. We compare in this section the performance of Gauss–Seidel algorithm and gmres algorithm.

A 3D case is presented where the reservoir, sideburden, overburden and underburden are gridded. Table III gives the dimensions of the reservoir and geomechanical domains and Figure 1 displays the mesh used to discretize the reservoir and the surrounding formations. The reservoir mesh (Figure 2) is composed of $21 \times 21 \times 3$ cells (1323 cells finite volume active cells), whereas the geomechanical mesh is made of a Cartesian grid of $27 \times 27 \times 14$ cells (10 206 finite element active cells) embedding the reservoir grid.

Table III. Dimension of the reservoir case.

Reservoir surrounding formations	Overburden thickness	2500 m
	Underburden thickness	750 m
	Lateral extension	4570 m
Reservoir	Areal extension	1525 m × 1525 m
	Thickness	50 m

DOI: 10.1002/nag

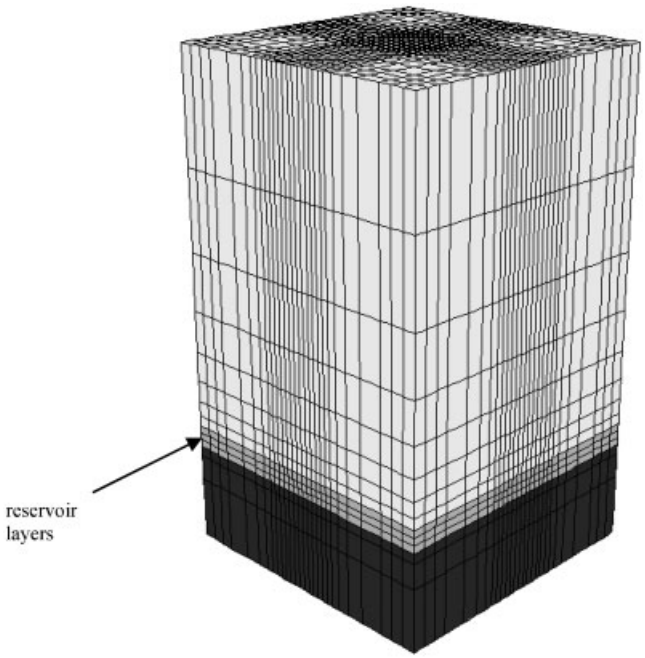

Figure 1. The mechanical mesh.

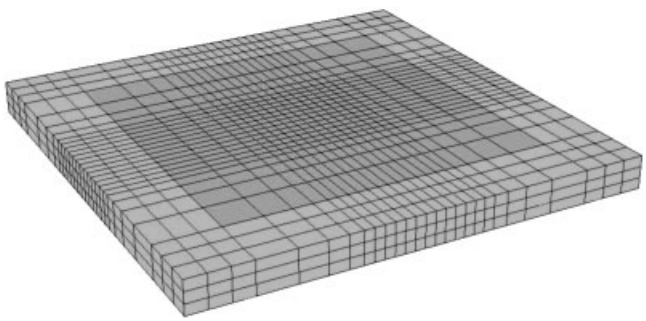

Figure 2. The reservoir mesh (dark grey cells) with sideburden.

The mechanical properties of the surrounding formations are given in Table IV.

Reservoir properties used for the stress simulation are given in Table V.

As the lateral boundaries of the geomechanical domain are set far from the reservoir zone, the normal displacements applied to the lateral boundaries are fixed at zero. The displacement vector at the bottom of the geomechanical model is also equal to zero. The initial stress state before reservoir production is obtained by computing the mechanical equilibrium of the model submitted to regional stress. Total vertical stress (σ_v) is determined by rock densities. The horizontal stresses (σ_H and σ_h) are given by an estimated stress ratio ($\sigma_h/\sigma_v = \sigma_H/\sigma_v = 0.7$). Accounting for the initial pore pressure issued from the reservoir simulation, the effective stresses are computed as the difference between total stresses and pore pressure. A computed

DOI: 10.1002/nag

Table IV. Mechanical properties of the surroundings formation.

	Rock density	$2600\,\mathrm{kg\,m^{-3}}$
Surrounding formations	Young's modulus of the sideburden and underburden	1.4×10^4 MPa
	Poisson ratio of the sideburden and underburden	0.25
	Young's modulus of the overburden	2×10^3 MPa
	Poisson ratio of the overburden	0.35

Table V. Properties of the reservoir (permeability curves are given in Appendix A).

	Oil density	$850\,\mathrm{kg\,m^{-3}}$
Fluid properties	Oil compressibility	$7.25 \times 10^{-10}\,\mathrm{Pa^{-1}}$
	Water density	$1000\,\mathrm{kg\,m^{-3}}$
	Water compressibility	$5 \times 10^{-10}\,\mathrm{Pa^{-1}}$
	Oil viscosity	1×10^{-3} Pa s
	Water viscosity	1×10^{-3} Pa s
Petrophysical properties	Porosity	0.36
	Permeability	$10^{-13}\,\mathrm{m^2}$
	Rock density	$2700\,\mathrm{kg\,m^{-3}}$
	Capillary pressure	Neglected
Mechanical properties	Rock density	$2640\,\mathrm{kg\,m^{-3}}$
	Drained Young's modulus	$2.4 \times 10^{+3}$ MPa
	Poisson ratio	0.30
	Biot's coefficient	1

initialization was performed to reach a mechanical equilibrium between the applied boundary conditions and the initial state of stress in the structure.

Continuity of displacement vector and the traction is imposed at the boundary between the reservoir and the surrounding formations.

The initial saturation in the reservoir is equal to the irreducible water saturation $S_{\mathrm{wi}} = 0.1$ and the initial pressure is 48.3 MPa.

Reservoir production is achieved by a set of producer wells located at the centre of the finite volume reservoir mesh producing in the three reservoir layers. The total rate of production is $1600\,\mathrm{m^3\,days^{-1}}$.

This production period is divided into four periods of three months. Each period of coupling is divided into a variable number of reservoir time steps.

The convergence criteria of the two iterative algorithms are now set to 10^{-4} for the relative variation in displacement between two consecutive iterations. We verified the accuracy of the results; the normalized L^{∞} norm of the relative difference of the pressure and displacement solution fields obtained by the two algorithms was lower than 10^{-3} at the end of the simulation. Table VI compares the mean number of stress simulations for the four coupling periods.

Although a relaxation parameter allows the staggered algorithm to converge, the rate of convergence remains slow compared to the non-linear gmres algorithm when a precision of 10^{-4}

DOI: 10.1002/nag

Table VI. Mean number of stress simulations of coupling periods for different algorithms.

	Staggered algorithm with oedometric compressibility	Non-linear gmres algorithm
Number of reservoir and geomechanical simulations per period of coupling	19-20-20-19	8-15-15-15

is chosen. for a lower precision of 10^{-2}, the performance of the algorithms are similar to this test case.

However, for some critical values of physical data, the performance of the Gauss–Seidel algorithm is really bad:

- if we increase the overburden stiffness (using a young's modulus of $1.4 \times 10^{+4}$ MPa), the number of iterations of the staggered algorithm is 1.8 times the gmres number of iterations for a precision of 10^{-4}. in this case the loading can no more be approximated by an oedometric path and both the relaxed staggered and the staggered algorithm converge slower than the gmres algorithm.
- if we consider a young's modulus as low as $2.4 \times 10^{+3}$ MPa in the reservoir (such weak value can mimic plastic behaviour [18]), the relaxed staggered algorithm does not converge, ever with a precision of 10^{-2}, whereas the gmres algorithm converges.

The two tests we consider in this section concern rocks with linear elastic behaviour. these algorithms are fully adapted in practical situations for which the geomechanical behaviour is non-linear, see e.g. [19, 20]; the problem remains a non-linear fixed point problem. the use of the Gauss–Seidel algorithm and gmres algorithm remains straightforward also with industrial simulators.

5. CONCLUSION

Different algorithms have been developed to solve the coupled fluid flow–elastic deformation problem with iterative methods. These methods consider the coupled problem as a non-linear fixed point problem and solve it using alternate resolution of a reservoir fluid flow problem and a mechanical problem. For linear reservoir simulation, the conventional staggered algorithm used in reservoir engineering can be interpreted as a Gauss–Seidel algorithm and can be highly improved when using a relaxation technique (the performance is however highly sensitive to the choice of the relaxation parameter). We study in this paper two other algorithms, the non-linear gmres and non-linear conjugate gradient, for the resolution of the coupled problem.

Several numerical tests were carried out on 1D and 3D structures, including performance comparisons. The non-linear gmres algorithm and the preconditioned gradient conjugate method are more robust than the relaxed staggered algorithm. The preconditioned conjugate gradient algorithm seems attractive: in spite of lack of robustness due to possible non-symmetry and positivity of the Jacobian matrix, this algorithm requires only one geomechanical simulation for two reservoir simulations. However, a drawback of this approach when using industrial simulators remains that the stiffness matrix A and the coupling matrix B have to be

DOI: 10.1002/nag

extracted from geomechanical and reservoir simulators. The non-linear gmres algorithm is a robust algorithm with interesting performance, particularly adapted to the resolution of non-linear coupling problem. Moreover, it can be used, as it is, for coupling problems with non-linear poro-mechanical constitutive law.

APPENDIX A

Water and oil relative permeabilities for the 3D reservoir production case are given in the following table:

S_w	K_{rw}	K_{row}
0.10	0.000000	1.000000
0.15	0.003086	0.826446
0.20	0.012346	0.669421
0.25	0.027778	0.528926
0.30	0.049383	0.404959
0.35	0.077160	0.297521
0.40	0.111111	0.206612
0.45	0.151235	0.132231
0.50	0.197531	0.074380
0.55	0.250000	0.033058
0.60	0.308642	0.008264
0.65	0.373457	0.000000

REFERENCES

1. Geertsma J. A basic theory of subsidence due to reservoir compaction: the homogeneous case. *Verhandelingen van het Koninklijk Nederlands Geologish Mijnbouwkundig Genootschap* 1973; **28**:22–43.
2. Biot MA. General theory of three-dimensional consolidation. *Journal of Applied Physics* 1941; **12**:155–164.
3. Settari A, Mourits FM. A coupled reservoir and geomechanical simulation system. *SPE Journal* 1998; **September**:219–226.
4. Settari A, Walters DA. Advances in coupled geomechanical and reservoir modeling with applications to reservoir compaction. *Proceedings of SPE reservoir Simulation Symposium*, Houston, Texas, 14–17 February 1999.
5. Settari A, Mourits FM. Coupling of geomechanics and reservoir simulation models. In *Computer Methods and Advances in Geomechanics*, Siriwardane HJ, Zeman MM (eds). Balkema: Rotterdam, 1994; 2151–2158.
6. Mainguy M, Longuemare P. Coupling fluid flow and rock mechanics: formulations of the partial coupling between reservoir and geomechanical simulators. *Oil and Gas Science and Technology* 2002; **57**(4):355–367.
7. Tran D, Settari A, Nghiem L. New iterative coupling between a reservoir simulator and a geomechanics module. *SPE Journal* 2004; **September**:362–369.
8. Daïm F, Eymard R, Hilhorst D, Mainguy M, Masson R. A preconditioned conjugate gradient based algorithm for coupling geomechanical-reservoir simulations. *Oil and Gas Science and Technology* 2002; **57**(5):515–523.
9. Coussy O. *Poromechanics*. Wiley: New York, 2004.
10. Eymard R, Gallouët T, Herbin R. The finite volume method. In *Handbook of Numerical Analysis*, Ciarlet PG, Lions JL (eds), vol. 7. Elsevier, 2000; 715–1022.
11. Lewis RW, Schrefler BA. *The Finite Element Method in the Static and Dynamic Deformation and Consolidation of Porous Media* (2nd edn). Wiley: New York, 1998.

DOI: 10.1002/nag

12. Loula AFD, Murad MA. Improved accuracy in finite element analysis of Biot's consolidation problem. *International Journal for Numerical Methods in Engineering* 1992; **95**:259–382.
13. Wan J. Stabilized finite element methods for coupled geomechanics and multiphase flow. *Ph.D. Thesis*, Stanford University, 2002.
14. Chin LY, Thomas LK. Fully coupled analysis of improved oil recovery by reservoir compaction. *Proceedings of SPE Annual Technical Conference and Exhibition*, Houston, Texas, 3–6 October 1999; 393–401.
15. Addis MA, Choi X, Gunning J. The influence of the reservoir stress-depletion response on the lifetime considerations of well completion design. *Paper SPE/ISRM 47289*, 1998.
16. Bévillon D, Masson R. Stability and convergence analysis of partially coupled schemes for geomechanical-reservoir simulations. *Proceedings of ECMOR VII 2000*, Baveno, Italy, September 2000.
17. Saad Y, Schultz MH. GMRES: a generalized minimum residual algorithm for solving nonsymmetric linear system. *SIAM Journal on Scientific and Statistical Computing* 1986; **7**:856–869.
18. Longuemare P. Couplage hydrodynamique pour les lois de comportement non linéaires. *Thèse de l'Université des Sciences et Techniques de Lille*, 1996.
19. Chin LY, Nagel NB. Modelling of subsidence and reservoir compaction under waterflood operations. *International Journal of Geomechanics* 2004; **4-1**:28–34.
20. Schrefler BA, Gens A, Simoni L. New data about surface subsidence above gas reservoirs, *Revue européenne de Génie Civil* 2005; **9**:817–825.

DOI: 10.1002/nag